buildings

MDPI

Article

Analysis of Hydration Mechanism of Steel Slag-Based Cementitious Materials under Saline–Alkaline-Coupled Excitation

Jianping Liu [1], Bing Liu [1], Xiaowei Ge [2,3,*], Yulin Tian [1], Ge Song [1], Kaixin Liu [1] and Yilin Wang [1]

[1] School of Architecture and Civil Engineering, Shenyang University of Technology, Shenyang 110870, China; liujianping024@163.com (J.L.); liubing19981101@163.com (B.L.); tyl417@gmail.com (Y.T.); 17602482397@163.com (G.S.); lll1684384756@163.com (K.L.); 15536306645@163.com (Y.W.)
[2] School of Resources and Civil Engineering, Northeastern University, Shenyang 110819, China
[3] Science and Technology Innovation Center of Smart Water and Resource Environment, Northeastern University, Shenyang 110819, China
* Correspondence: 2310425@stu.neu.edu.cn

Abstract: In order to realize the resourceful, large-scale, and high-value utilization of steel slag, which is a bulk industrial solid waste, and to reduce the use of cement-based cementitious materials, this study adopted the coupled excitation effect of sodium carbonate–magnesium oxide–desulfurization gypsum to excite steel slag-based cementitious materials, and it preliminarily investigated the hydration process of the steel slag-based cementitious system by the analysis of the heat of hydration of the cementitious materials and the pH value of the pore solution. The hydration products and microscopic morphology of the steel slag-based gelling material were initially investigated by XRD and SEM technical means on the gelling system. The results showed that the hydrolysis of the exciter and the dissociation of the active components in the steel slag provided an alkaline environment and relevant ions for the gelling system, which promoted the generation of the AFt and hydrotalcite phases. Subsequently, the AFt provided ungenerated sites for C-S-H gels as well as calcites, and the hydrotalcite phase accelerated the transformation of the carbonate phase in the gelling system, which promoted the synergistic effect of the hydration of the steel slag and mineral slag. Eventually, a large number of C-S-H gels, calcites, and other hydration products were generated in the gelling system under the synergistic effect of the hydration of the steel slag and slag, which was manifested in the improvement in the mechanical properties at the macrolevel. In addition, this study also standardized 28 d steel slag-based gelling for carbonization maintenance, and the data show that a carbonization temperature of 70 °C, CO_2 pressure of 0.7 MPa, and carbonization time of 30 min achieved the best results, with a strength of up to 51.22 MPa, illustrating that steel slag-based gelling materials are safe and can be used for the green storage of CO_2.

Keywords: steel slag; hydration stack effect; hydration mechanism; hydration products; microstructure; carbonation maintenance

check for updates

Citation: Liu, J.; Liu, B.; Ge, X.; Tian, Y.; Song, G.; Liu, K.; Wang, Y. Analysis of Hydration Mechanism of Steel Slag-Based Cementitious Materials under Saline–Alkaline-Coupled Excitation. *Buildings* **2024**, *14*, 597. https://doi.org/10.3390/buildings14030597

Academic Editor: Marco Di Ludovico

Received: 17 January 2024
Revised: 14 February 2024
Accepted: 20 February 2024
Published: 23 February 2024

Copyright: © 2024 by the authors. Licensee MDPI, Basel, Switzerland. This article is an open access article distributed under the terms and conditions of the Creative Commons Attribution (CC BY) license (https://creativecommons.org/licenses/by/4.0/).

1. Introduction

Steel slag is a gray-black solid waste produced in the steelmaking process, and its output rate is about 15% of steel production [1,2]. At present, most enterprises cannot carry out the timely treatment of steel slag, resulting in a large number of random accumulations of steel slag, resulting in a certain degree of environmental damage and waste of resources [3,4]. Even when steel slag is used as an aggregate and filler material in concrete and roadbed pavement projects, the actual utilization rate is only about 30%; thus, the resource utilization of steel slag is urgent [5–7].

The main chemical compositions of steel slag and cement are shown in Table 1. From Table 1, it can be seen that the chemical composition of steel slag is very similar to the

composition of cement [8,9]. However, steel slag contains a large number of low-activity γ-C_2S, as well as FeO, MgO, and MnO in the high-temperature action of the RO phase formed by melting, both of which affect the activity of the steel slag to a certain extent; thus, a certain amount of steel slag mixed with a higher activity of solid waste can be considered to improve the conditions of its preservation and achieve its resourceful use [10–12]. Blast-furnace slag, as a glassy calcium–aluminum silicate by-product with potential hydration activity produced in the process of blast-furnace ironmaking, needs to be used with alkaline exciters to dissolve the protective film of the silica–aluminum silicate on its surface and release the active metal cations inside [13–15]. Although the compounding of sodium hydroxide and water glass can solve this problem, it has the disadvantages of high cost and high risk [16]. The use of sodium carbonate, magnesium oxide, and gypsum can avoid these problems [17,18]. At the same time, steel slag contains a large number of γ-C2S, which, under a certain pressure, temperature, and time, can be reacted with CO_2 and have high activity (the detailed reaction equations are shown in Equations (1) and (2)), also known as the carbonization of steel slag maintenance [19,20].

$$CO_2 + H_2O \rightarrow H_2CO_3 \quad (1)$$

$$\gamma\text{-}C_2S + H_2CO_3 \rightarrow 2CaCO_3 + SiO_2(gel) + 2H_2O \quad (2)$$

In summary, we can consider the following question: is it possible to mix a certain amount of steel slag in slag and use carbonization maintenance under the premise of sodium carbonate, magnesium oxide, and desulfurization gypsum as a three-compound exciter? This not only realizes the resourceful utilization of steel slag but also the safe and green storage of CO_2. Therefore, this study started from the coupled excitation effect of sodium carbonate–magnesium oxide–desulfurization gypsum and analyzed the hydration process of the cementitious material through the heat of hydration and the pH value of the pore solution. The hydration products and microscopic morphologies of the cementitious materials were analyzed by XRD and SEM technical means, and the hydration mechanism of the steel slag-based cementitious materials was preliminarily analyzed. In addition, the carbonization maintenance of steel slag-based cementitious materials was also carried out to study the effects of the carbonization temperature, CO_2 pressure, and time on the mechanical properties of the cementitious materials, so as to provide theoretical references for the resource utilization of steel slag in the future.

Table 1. The main chemical compositions of cement and steel slag.

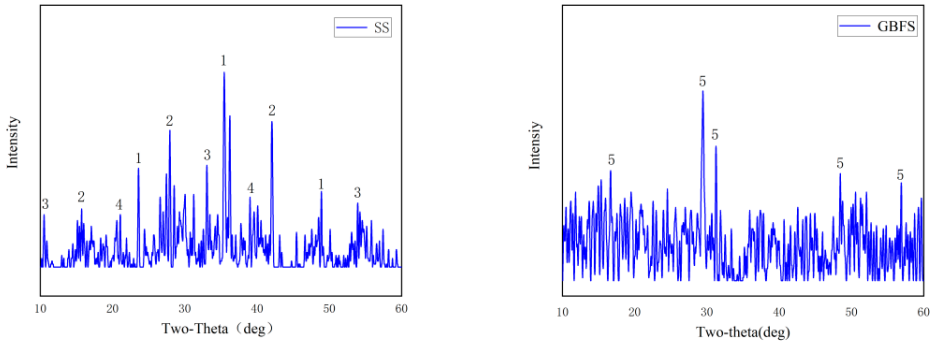
	CaO	**SiO_2**	**Al_2O_3**	**Fe_2O_3**	**MgO**	**FeO**	**P_2O_5**
Cement	62–68	20–24	4–7	2.5–6.5	1–2	—	trace
Steel slag	30–55	8–20	1–6	3–9	3–13	7–20	1–4

2. Experimental Materials and Methods

2.1. Raw Materials

The origins of the steel slag and slag were Zhengzhou City, Henan Province, and Yingkou City, Liaoning Province, respectively. The materials were firstly mechanically ground in the laboratory by ball mill and then analyzed for their mineral compositions by XRD; the results are shown in Figure 1. The figure illustrates that the mineral-phase composition of the steel slag primarily consisted of the C_2S, C_3S, C_2F, and RO phases. In contrast, the mineral-phase composition of the slag was mainly calcium–aluminum yellow feldspar, with the chemical molecular formula of $CaO\text{-}Al_2O_3\text{-}SiO_2$. At 60 min after the steel slag was milled, desulfurization gypsum was added to it, and it was then mixed and milled for another 20 min to ensure that the desulfurization gypsum had an effect on the chemical activation of the steel slag micropowder and the mineral phase of the slag. For the chemical activation of the steel slag micropowder, the gypsum used was construction gypsum from a company in Shenyang [21–23]. Table 2 shows the chemical compositions of the steel slag,

slag, magnesium oxide, and desulfurization gypsum, as determined by X-ray fluorescence spectrometry (XRF). The magnesium oxide used was from a company in Yingkou, Liaoning Province, the sodium carbonate was from a company in Jiaxing, Zhejiang Province, and the purity was analytically pure. The water-reducing agent was the Nai system water-reducing agent from a company in Shanghai.



(**a**) (**b**)

1—C_2S 2—C_3S 3—C_2F 4—RO phase 5—Cacoclasite ($2CaO{\cdot}Al_2O_3{\cdot}SiO_2$)

Figure 1. XRD patterns of steel slag and slag: (**a**) steel slag; (**b**) slag.

Table 2. Main chemical compositions of steel slag, slag, magnesium oxide, and desulfurization gypsum (W/%).

Material Science	SiO_2	Al_2O_3	Fe_2O_3	MgO	CaO	SO_3
Steel slag	16.75	3.87	20.12	7.35	41.74	
Slag	34.5	17.7	1.03	6.01	34	1.64
Magnesium oxide	7.09	0.38	0.28	85.09	2.35	
Desulfurization gypsum	4.3	3.1	31.97	0.18	0.33	51.84

2.2. Test Methods

2.2.1. Sample Mixing Ratios

Under the premise of fixing the constant dosage of sodium carbonate–magnesium oxide–desulfurization gypsum, the steel slag dosage (0%, 20%, 40%, 60%, and 80%) was taken as the variable to carry out a one-way influence test on the whole steel slag-based gelling system. The ratio of water to dry materials (including the steel slag, slag, desulfurization gypsum, magnesium oxide, sodium carbonate, and water reducer) was fixed at 0.32, and the specific operation procedure involved mixing the dry material powder in the mortar mixer for 3 min to ensure the homogeneity of the mixed powder, and then adding the sodium carbonate solution with a concentration of 10% and water. After mixing and stirring for 3 min, the standard sand was added in accordance with the ratio of rubber to sand (1:2), and then rapid mixing and stirring were carried out for 1 min and 30 s. The homogeneous mortar was poured in two layers into the 40 mm × 40 mm × 160 mm rectangular molds, the vibration table was used to vibrate them for 60 s to eliminate the voids, and then the samples were covered with plastic wrap to avoid water loss. The samples were carefully demolded after 48 h. The specific design of the mixing ratio test is shown in Table 3. The numbers in the test block numbers in the table are the steel slag dosages.

Various factors can affect the carbonation effect of steel slag-based cementitious materials. For example, differences in the chemical composition and mineral phases of steel slag can lead to differences in the carbonation effect. The increase in the carbonization temperature will not only affect the carbon dioxide diffusion rate, calcium ion solubility, and hydration reaction rate, but it will also lead to a reduction in the carbon dioxide solubility. The increase in the carbon dioxide pressure during carbonization has a positive effect on the diffusion rate of the carbon dioxide and the generation of the carbonate phase. This paper explores the carbonization effect of steel slag-based cementitious materials mainly

from three aspects: the carbonization temperature, carbonization time, and carbon dioxide pressure. The specific test program is shown in Table 4.

Table 3. Design table for different steel slag dosages and mixing ratio test.

Number	Steel Slag	Slag	Gypsum	$CaCO_3$	Mgo	Water Reducer	Water-to-Gel Ratio
G0	0	93%	7%	2%	7%	0.30%	0.32
G20	20%	73%	7%	2%	7%	0.30%	0.32
G40	40%	53%	7%	2%	7%	0.30%	0.32
G60	60%	33%	7%	2%	7%	0.30%	0.32
G80	80%	13%	7%	2%	7%	0.30%	0.32

Table 4. Experimental design of the effects of different influencing factors on the carbonization of the steel slag-based cementitious materials.

Number	Temp (°C)	CO_2 Pressure (MPa)	Time (min)
T-30	30	0.5	30
T-50	50	0.5	30
T-70	70	0.5	30
T-90	90	0.5	30
P-0.1	70	0.3	30
P-0.5	70	0.5	30
P-0.7	70	0.7	30
P-1.0	70	1	30
t-30	70	0.7	30
t-60	70	0.7	60
t-120	70	0.7	120
t-240	70	0.7	240

2.2.2. Carbonation Conservation

Combined with the results of the previous tests, the steel slag-based cementitious materials were first maintained to the specified ages, so that more active components of the cementitious system fully reacted, and they were then placed in the carbonization reactor. The apparatus mainly consists of a reaction kettle, carbon dioxide gas tank, and vacuum pump. Firstly, the kettle was pumped to vacuum by the vacuum pump to prevent air from interfering with the carbonization effect. Then, CO_2 gas with a 99.9% concentration was introduced, and the pressure and temperature in the kettle were controlled by a CO_2-pressure-reducing valve and a programmable thermostat. Finally, the mechanical properties were tested after the specified time.

2.2.3. Strength Testing

Mortar specimens with dimensions of 40 mm × 40 mm × 160 mm and net mortar specimens with dimensions of 40 mm × 40 mm × 40 mm were first cast. The strength tests were then carried out after curing at a temperature of 20 ± 1 °C and a humidity of more than 95% for the specified ages (3 d and 28 d).

2.2.4. Exothermic Hydration Test

An isothermal calorimeter was used to monitor the exothermic process of the hydration of the steel slag-based gelling material by first maintaining the test temperature at 20 °C ± 0.5 °C and then rapidly pouring the gelling material into the isothermal calorimeter.

2.2.5. XRD Analysis

Internal fragments of the steel slag-based cementitious materials of the specified ages were selected, and their hydration reactions were terminated with aqueous ethanol so that their mineralogical compositions could be analyzed again by X-ray diffractometry (XRD).

2.2.6. SEM Analysis

After selecting internal fragments of steel slag-based cementitious materials of specified ages and terminating their hydration reactions with aqueous ethanol, micrographs of the hardened slurries were observed using scanning electron microscopy (Sigma 300, Carl Zeiss AG, Oberkochen, Germany).

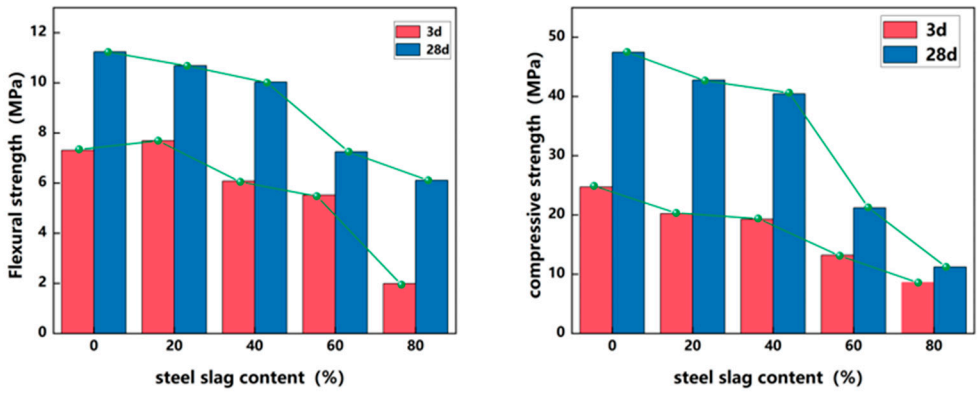
2.2.7. Determination of the pH of the Pore Solution

Under the premise of standard maintenance, 10 g of cementitious material was placed into a conical flask, and then 50 mL of ultrapure water was added to determine the pH value of the upper layer of the clear liquid at different reaction ages.

3. Strength Development and Carbonation Effect of Steel Slag-Based Cementitious Materials

3.1. Strength Development

Figure 2 and Table 5 show the effects of the steel slag dosages on the mechanical properties of the steel slag-based cementitious materials. The results show that there is an inverse relationship between the amount of steel slag and its mechanical properties. In particular, the 28-day compressive strength was only 11.22 MPa at the 80% steel slag dosage. This is because steel slag contains a large number of RO phases and low-activity γ-C_2S, and its hydration reaction will be changed from slag-dominated to steel slag-dominated when the dosage of steel slag is too high in the cementitious system, thereby affecting its mechanical properties [24,25]. Meanwhile, the 28-day compressive strength decreased from 47.47 MPa to 42.77 MPa when the dosage of steel slag was increased from 0% to 20%, with a decrease of 10.98%. When the dosage of steel slag was increased from 20% to 40%, the 28-day compressive strength decreased from 42.77 MPa to 40.77 MPa, with a decrease of only 5.67%. When the dosage of steel slag reached 60%, the strength decreased rapidly, and the 28 d compressive strength decreased from 40.44 MPa to 21.22 MPa, with a decrease of up to 47%. This shows that the steel slag dosage at 40% can produce a certain hydration synergistic effect with slag, offsetting some of the effects of the steel slag in the RO phase and low-activity γ-C_2S on the mechanical properties of the cementitious materials.



(**a**) (**b**)

Figure 2. Effects of steel content on mechanical properties of cementitious materials: (**a**) flexural strength; (**b**) compressive strength.

Table 5. Strengths at different ages of specimens with different steel slag dosages.

Steel Slag Content	Flexural Strength (Mpa)		Compressive Strength (Mpa)	
	3 d	28 d	3 d	28 d
0	7.31	11.23	24.72	47.47
20%	7.69	10.68	20.22	42.77
40%	6.08	10.03	19.28	40.44
60%	5.52	7.25	13.21	21.22
80%	1.99	6.11	8.62	11.22

3.2. Carbonization Conservation Effect

Table 6 and Figure 3 present the influences of different factors on the mechanical properties of G40, of which Figure 3a indicates the influence law of the carbonization temperature on the compressive strength of G40. In Figure 3a, it can be seen, regardless of whether at 3 d or 28 d, that the two changes in the trend of the compressive strength are basically the same: first an improvement and then a reduction. At the maintenance age of 28 d, when the carbonization temperature was 70 °C, the compressive strength was higher (16.2%) than that at the carbonization temperature of 30 °C, and when the carbonization temperature reached 90 °C, the gelling material appeared to decline, compared with 7 °C, when it decreased by 13.45%.

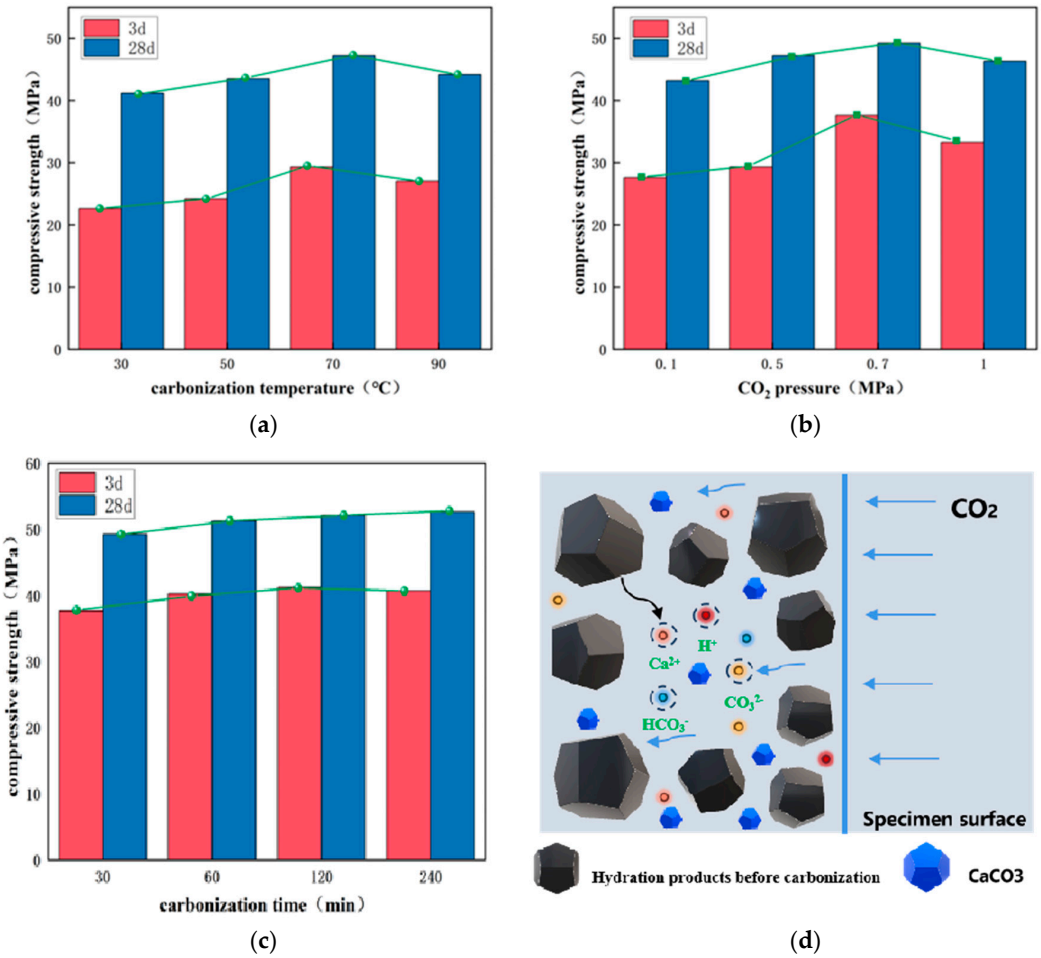


Figure 3. Carbonization effects and carbonization mechanisms of different factors on steel slag-based cementitious materials: (**a**) carbonization temperature; (**b**) carbonation pressure; (**c**) carbonization time; (**d**) carbonation mechanism.

Table 6. Carbonization effects of different influencing factors on steel slag-based cementitious materials.

Number	Temperature (°C)	CO_2 Pressure (MPa)	Time (min)	Compressive Strength (MPa)	
				3 d	28 d
T-30	30	0.5	30	22.64	41.22
T-50	50	0.5	30	24.21	43.52
T-70	70	0.5	30	29.32	47.25
T-90	90	0.5	30	27.04	44.21
P-0.1	70	0.3	30	27.63	43.21
P-0.5	70	0.5	30	29.32	47.25
P-0.7	70	0.7	30	37.63	49.24
P-1.0	70	1	30	33.27	46.31
t-30	70	0.7	30	37.63	49.24
t-60	70	0.7	60	40.22	51.22
t-120	70	0.7	120	41.21	52.05
t-240	70	0.7	240	40.68	52.58

The main reason for this phenomenon is that the carbonation temperature is directly proportional to the rate of carbon dioxide diffusion and the hydration reaction rate of the cementitious system, which generates more carbonate precipitate (the main component is $CaCO_3$) carbonate, which can fill the pores of the cementitious system, reduce the porosity, and thereby make the structure denser, which improves the mechanical properties of the cementitious system (as shown in Figure 3d) [19]. When the carbonation temperature reaches 90 °C, the carbon dioxide solubility will not only reduce the water in the cementitious system but will also cause the rapid evaporation of water in the cementitious system; in the above two cases, in the macro-performance of the cementitious material, the mechanical properties decline [20].

Figure 3b presents the influence law of the carbon dioxide pressure on the compressive strength of G40. In Figure 3b, it can be seen that, at the age of 28 d, the two compressive-strength change trends are basically the same: first an improvement and then a reduction. At the maintenance age of 28 d, the compressive strength was 13.96% higher at the carbonation pressure of 0.7 MPa than that at the carbonation pressure of 0.1 MPa, and when the carbonation pressure reached 1 Mpa, the gelatinized material appeared to decline, compared with 70 °C, when it decreased by 7.82%.

This is because the carbon dioxide pressure is proportional to the leaching efficiency of the relevant ions in G40, which promotes the generation of hydration products, such as C-S-H gels, calcites, and magnesites. This is manifested macroscopically in the enhancement of the mechanical properties. It is worth noting that G40 showed a decrease in strength at a CO_2 pressure of 1 MPa. This is because the carbonation reaction was "from the outside to the inside" step by step, and a too-high carbon dioxide pressure will make the reaction too fast in the cementitious material surface and generate a layer of dense "protective film". Although the existence of the protective film will reduce the porosity and improve the mechanical properties of the cementitious system, it will also prevent the further diffusion of carbon dioxide, hindering the further carbonization reaction within the cementitious system (as shown in Figure 4) [26,27].

Figure 3c shows the influence of the carbonization time on the compressive strength of G40, where the carbonization time of 60 min at age 28 d shows a small increase in strength of 4.02% compared to that at 30 min. Therefore, considering the above factors, the carbonization condition of G40 is most suitable when the carbonization temperature is 70 °C, the carbon dioxide pressure is 0.7 MPa, the carbonization time is 30 min, and the compressive strength is 51.22 MPa.

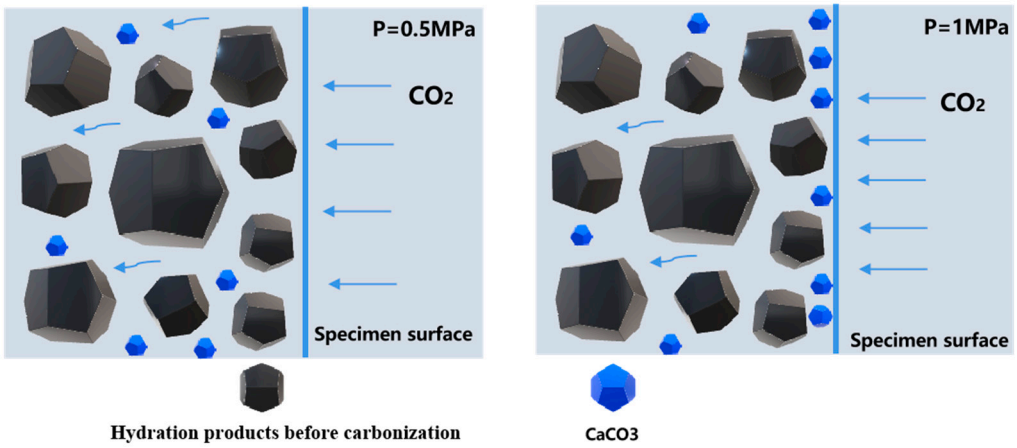


Figure 4. Schematic diagram of mechanism of carbon dioxide pressure on carbonization of steel slag-based cementitious materials.

4. Hydration Process of Steel Slag-Based Cementitious Materials

4.1. Heat of Hydration

According to the influence of steel slag doping on the strength of the steel slag-based cementitious materials, comparing G60 and G40, there was up to a 47% decline in the strength. An isothermal calorimeter was used to measure the heat of hydration of the steel slag-based cementitious materials at G40, as shown in Figure 5, where it can be observed that there are three major exothermic peaks of the exothermic curve of the steel slag-based cementitious materials.

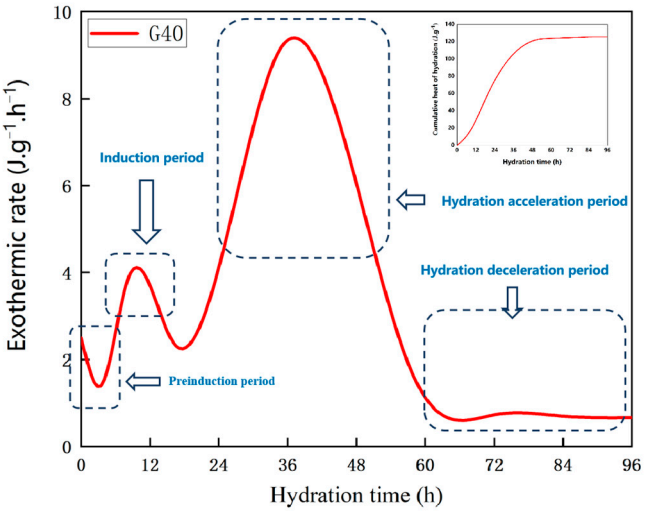


Figure 5. Hydration exothermic rate and cumulative exothermic amount of cementitious system with 40% steel slag dosage.

The first exothermic peak occurs due to the dissociation of steel slag from slag and the ionization that occurs when the chemical exciters come into contact with water. The second exothermic peak occurs in the range of 4–10 h and is characterized as small and short. It is hypothesized that this is related to the generation of calcite and AFt in the gelling system [28–31]. The third exothermic peak appears after 24 h, which is characterized by a significant long exothermic duration, and it is presumed that this is related to the generation of C-S-H gel, calcite, and the hydrated fossil phase in the gelling system [32,33]. Combined with the above conclusions, it can be speculated that the exothermic process of steel slag and slag under the coupled excitation of sodium carbonate–magnesium oxide–desulfurization gypsum can be divided into a pre-induction period, an induction period, a hydration acceleration period, and a hydration deceleration period [34]. To better understand the

hydration reactions in the different stages of steel slag-based cementitious materials and reveal the underlying mechanism, we conducted additional studies using the pore liquid pH, XRD, and SEM.

4.2. Pore Solution Analysis

As shown in Figure 6, the dosage of steel slag is directly proportional to the pore liquid pH, and the pore liquid pH increases and then decreases with the increase in the reaction age. The reason for this phenomenon is that the addition of steel slag and a chemical exciter enhances the alkalinity of the cementitious system, making the pore fluid pH larger in the first two hours. And subsequently, as the dissociation equilibrium of the steel slag is broken, the hydroxide ions and calcium ions in the gelling system are consumed so that a C-S-H gel is generated in the gelling system, which reduces the pore fluid pH [35]. The reason for the decrease in the pH in the later stage is that the hydration products encapsulate the unhydrated steel slag and slag particles, which hinders the generation of C-S-H gel and the consumption of hydroxide ions and thereby raises the pH of the pore fluid.

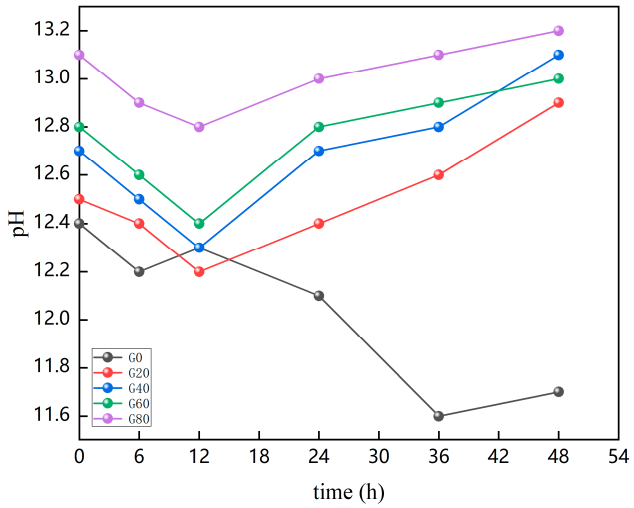


Figure 6. Effects of steel slag dosages on pore fluid pH value.

5. Hydration Products of Steel Slag-Based Cementitious Materials

5.1. XRD Analysis

As shown in Figure 7, the main diffraction peaks of the hydration products of the steel slag-based cementitious materials with different steel slag dosages were the desulfurized gypsum phase, AFt phase, calcium hydroxide phase, calcite phase, and hydrotalcite phase. The calcium hydroxide diffraction peaks appear because steel slag contains a large amount of calcium oxide, which reacts with water to form calcium hydroxide (see Equation (3)). The appearance of desulfurization gypsum and AFt diffraction peaks is because the addition of desulfurization gypsum introduces sulfate ions, and the sulfate ions can be dissociated with the slag meta-aluminate ions reacted to form AFt (see Equations (4)–(6)), and when the amount of slag mixing is too small, the slag dissociation of the meta-aluminate is insufficient, which will affect the generation of calcite crystals [36]. Calcite appears because the addition of sodium carbonate introduces carbonate ions into the gelling system, which generate calcium carbonate with calcium ions in the gelling system, and calcium carbonate exists in the gelling system as the main component of calcite. The appearance of the hydrographite phase is because magnesium oxide can react with water to form the hydrographite phase, the magnesium ions in the hydrotalcite phase are replaced by aluminum ions with similar radii, and the hydrotalcite phase is formed under the action of carbonate ions and other factors [37].

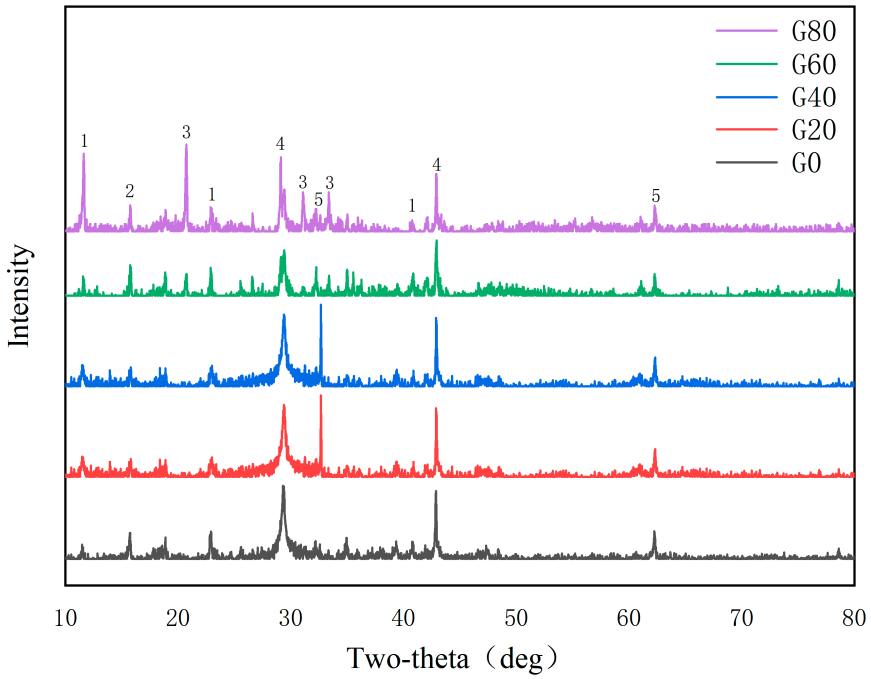
$$CaO + H_2O = Ca(OH)_2 \quad (3)$$

$$[AlO_2{}^- + 2OH^- + 2H_2O = [Al(OH)_6]^{3-} \quad (4)$$

$$[Al(OH)_6]^{3-} + 6Ca^{2+} + 24H_2O = \{Ca_6[Al(OH)_6]_2 \cdot 2H_2O\}^{6+} \quad (5)$$

$$\{Ca_6[Al(OH)_6]_2 \cdot 24H_2O\}_6 + + 3SO_4{}^{2-} + 2H_2O = \{Ca_6[Al(OH)_6]_2 24H_2O\}\ [3SO_4{}^{2-} \cdot 2H_2O] \quad (6)$$

It is worth noting that G20 and G40 have strong hydrotalcite-phase diffraction peaks, while the hydrotalcite-phase diffraction peaks of G60 show a decrease in intensity, which is due to the fact that the hydration reaction of the cementitious system is dominated by the steel slag at the beginning of the reaction, which leads to an insufficient concentration of meta-aluminate ions in the cementitious system, which affects the generation of the hydrotalcite phase [34]. The hydrotalcite phase has the effect of accelerating the transformation of the carbonate phase in the gellant, and this explains why the intensity of the calcite diffraction peak in the gellant system decreases when the dosage of steel slag exceeds 40% [33], which, in turn, explains the rapid decrease in the mechanical properties of the gelling agent when the dosage of steel slag exceeds 40%.



1—Desulfurization gypsum; 2—Aft; 3—Ca(OH)2; 4—Calcite; 5—hydrotalcite

Figure 7. XRD diffractograms of steel slag-based cementitious materials with different steel slag dosages.

5.2. SEM Analysis

The SEM of the steel slag-based cementitious materials at the age of 28 days and the dosages of steel slag of 40% and 60% are shown in Figure 8, from which it can be seen that the structure of G60 compared with that of G40 has obviously become loose and has obvious cracks, some of the generated calcium alumina crystals are exposed, there is no overlap or interlocking with the C-S-H gels to form a dense structure, and it is macroscopic and manifested as a decline in the mechanical properties of the steel-slag-based cementitious materials.

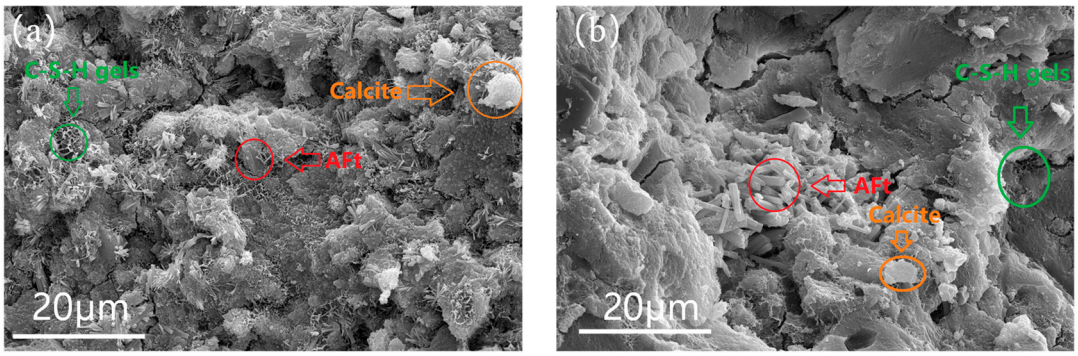


Figure 8. SEM images of steel slag-based cementitious materials with different steel slag dosages: (**a**) G40; (**b**) G60.

In addition, it can be seen from Figure 9 that, at 3 d, the generation of calcite provided generating sites for the subsequent generation of calcite and C-S-H gels. With the increase in age, calcite and C-S-H gels were generated in large quantities and overlapped and interspersed with AFt, which enhanced the mechanical properties of the gelling system [38,39]. In addition, the generation of the hydrated fossil phase plays a role in accelerating the transformation of the carbonate phase in the cementitious system, such as the transformation of oblique soda-lime to calcite, which improves the late strength of the cementitious system.

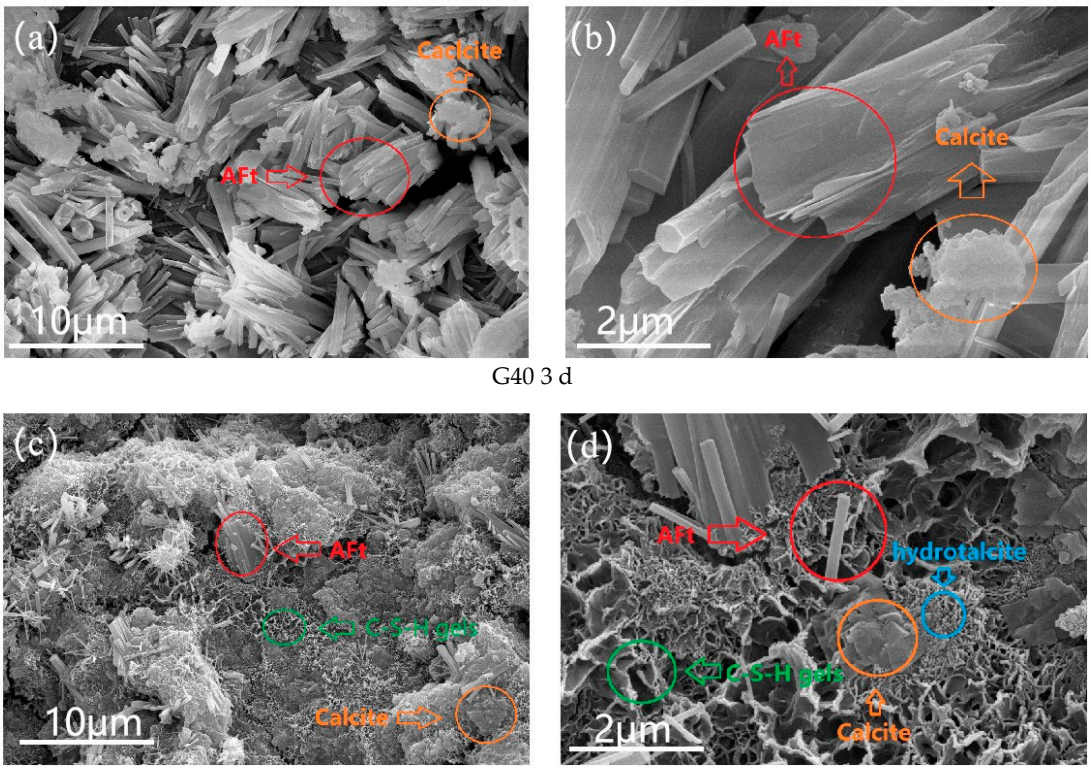


Figure 9. SEM images of steel slag-based cementitious materials at 3 d and 28 d with 40% steel slag: (**a**,**b**); G40-3 d, (**c**,**d**); G40-28 d.

6. Hydration Mechanism Analysis

Combined with the above experimental results, the heat-of-hydration curves of steel slag-based cementitious materials are described as follows: (1) the pre-induction period: this period is dominated by the hydrolysis of the chemical exciters and the dissociation of the steel slag and slag, which leads to an increase in the concentration of the relevant

ions in the system and an increase in the pH of the gelling system; (2) the induction period: the increasing alkalinity in the gelation system and the introduction of metal active cations and sulfate ions lead to the precipitation of AFt crystals, which provide a site for the subsequent generation of C-S-H gel and calcite [4]; (3) the hydration acceleration period: as the hydration reaction proceeds, the dissolution equilibrium of the slag is broken, and the synergistic effect of steel slag and slag begins to appear, prompting the generation of a large number of C-S-H gels with calcite; (4) the hydration deceleration period: the slowing down of the curvature of the hydration exothermic curve indicates that the generated hydration products encapsulate the unreacted steel slag and slag, which affects the subsequent reaction.

Therefore, the hydration process of steel slag-based cementitious materials can be initially divided into four stages: mineral-phase dissociation, AFt generation, slag dissociation, and structural hardening (as shown in Figure 10).

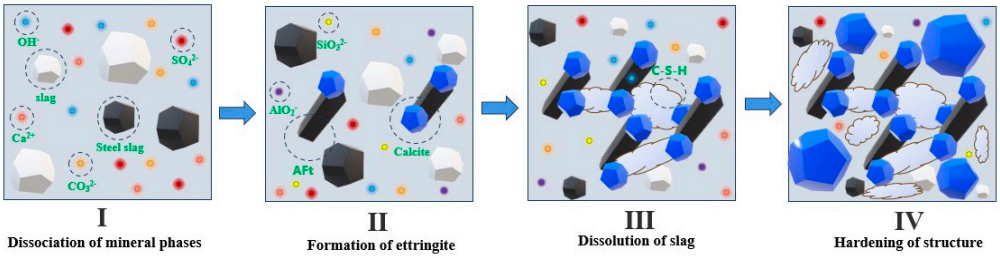


Figure 10. Hydration mechanism of steel slag-based cementitious materials.

The first stage mainly consists of the ionization of the chemical exciters and the dissociation of the more active mineral phases in the steel slag and slag, so that the concentration of hydroxide ions, calcium ions, magnesium ions, and other related ions in the system increases significantly, providing alkaline conditions and related ions for the subsequent hydration reaction. In terms of the hydration reaction, hydration into the second stage (that is, the generation of calcium alumina and the hydrotalcite phase), this period is mainly due to the slag at the surface of the aluminosilicate protective film that plays a role in the dissolution of hydroxide ions, so that it is wrapped in the silica-rich phase in which there is full contact with hydroxide ions, so that it releases a large number of silica–oxygen tetrahedra and aluminum–oxygen tetrahedra. At the same time, in terms of the role of hydroxide ions, magnesium ions participate in the formation of hydrated fossil-like phases and hydromagnesite, and sulfate ions are involved in the formation of calcite. The former provides sites for the generation of C-S-H gels and calcite, and the latter accelerates the transformation of the carbonate phases and promotes the generation of calcite [4]. In addition, as the hydration reaction proceeds, the hydration enters the third stage. Due to the dissociation of the silica–oxygen tetrahedra of the slag, the silica–oxygen bond is transformed into silicate ions, and the alkaline environment absorbs a large number of calcium ions while reducing the concentration of calcium ions in the system, which induces the dissociation of the steel slag and maintains the alkalinity of the hydration reaction slurry at a certain level. The maintenance of the alkalinity of the gelling system prompts the further deepening of the dissociation of the slag, generating a large number of C-S-H gels filled in the gelling system. With the continuous consumption of the steel slag and slag, a large number of hydration products are generated and ultimately wrapped around the unhydrated steel slag and slag, affecting the subsequent hydration reaction, but the unhydrated steel slag and slag also play a role in filling, so that the structure is denser. The further improvement in the mechanical properties at this stage is called hardening.

7. Conclusions

(1) Under the condition of saline–alkaline-coupled excitation, the ratio of slag, steel slag, and desulfurization gypsum was 53:40:7, and the late mechanical properties of the cementitious material decreased the least (only 5.67%, and the 28 d compressive

strength was 40.44 MPa). This indicates that a steel slag dosing of 40% can produce the best hydration synergy with the slag, offsetting some of the effects of the steel slag in the RO phase and the low-activity γ-C_2S on the mechanical properties of the cementitious materials;

(2) When the steel slag-based cementitious materials were standardized to 28 d and then placed at a carbonization temperature of 70 °C, a CO_2 pressure 0.7 MPa, and a carbonization time of 30 min, the carbonization effect was the most appropriate, with a strength of up to 51.22 MPa;

(3) The addition of desulfurization gypsum enables the system to generate AFt to provide sites for the subsequent generation of C-S-H gels with calcite, while the addition of low-activity magnesium oxide can generate a hydrotalcite-like phase. The latter can play a role in accelerating the transformation of the steel carbonate phase;

(4) For the initial hydration mechanism of the gelling system, first, the hydrolysis of the chemical exciters provides an alkaline environment and associated ions for the gelling system, which promotes the generation of the AFt and hydrotalcite phases. Subsequently, AFt provides a site for the generation of C-S-H gels and calcite, while the hydrotalcite phase accelerates the transformation of the carbonate phase in the gelling system, promoting a synergistic effect on the hydration of the steel slag and slag. Eventually, under the synergistic effect of steel slag and slag hydration, a large number of C-S-H gels, calcites, and various other hydration products are generated in the gelling system, thereby improving the mechanical properties of the gelling materials.

Author Contributions: Formal analysis, J.L.; Data curation, X.G., Y.T., G.S., K.L. and Y.W.; Writing—original draft, B.L.; Writing—review & editing, J.L.; Supervision, J.L.; Funding acquisition, J.L. All authors have read and agreed to the published version of the manuscript.

Funding: This research was funded by the National Key Research and Development Plan of China, grant number 2023YFC3904303, the National Natural Science Foundation of China, grant number 52234004, and the Social Governance Special Project of Shenyang Municipal Bureau of Science and Technology, grant number 22-322-3-02.

Data Availability Statement: Data will be made available upon request due to privacy.

Acknowledgments: Special thanks to the Shiyanjia Lab (www.shiyanjia.com, accessed on 16 October 2023) for providing technical analysis.

Conflicts of Interest: The authors declare that they have no known competing financial interests or personal relationships that could appear to influence the work reported in this paper.

References

1. Jiang, Y.; Ling, T.C.; Shi, C.; Pan, S.Y. Characteristics of steel slags and their use in cement and concrete—A review. *Resour. Conserv. Recycl.* **2018**, *136*, 187–197. [CrossRef]
2. Zhao, J.; Yan, P.; Wang, D. Research on mineral characteristics of converter steel slag and its comprehensive utilization of internal and external recycle. *J. Clean. Prod.* **2017**, *156*, 50–61. [CrossRef]
3. Zhuang, S.; Wang, Q. Inhibition mechanisms of steel slag on the early-age hydration of cement. *Cem. Concr. Res.* **2021**, *140*, 106283. [CrossRef]
4. Gu, X.; Wang, H.; Liu, J.; Zhu, Z.; Wang, S.; Xu, X. Synergistic effects of steel slag and metakaolin in cementitious systems: Packing properties, strength, and microstructure. *Constr. Build. Mater.* **2024**, *411*, 134395. [CrossRef]
5. Fisher, L.V.; Barron, A.R. The recycling and reuse of steelmaking slags—A review. *Resour. Conserv. Recycl.* **2019**, *146*, 244–255. [CrossRef]
6. Brand, A.S.; Roesler, J.R. Steel furnace slag aggregate expansion and hardened concrete properties. *Cem. Concr. Compos.* **2015**, *60*, 1–9. [CrossRef]
7. Gao, T.; Dai, T.; Shen, L.; Jiang, L. Benefits of using steel slag in cement clinker production for environmental conservation and economic revenue generation. *J. Clean. Prod.* **2021**, *282*, 124538. [CrossRef]
8. Guo, J.; Bao, Y.; Wang, M. Steel slag in China: Treatment, recycling, and management. *Waste Manag.* **2018**, *78*, 318–330. [CrossRef] [PubMed]

9. Li, Z.; Zhao, S.; Zhao, X.; He, T. Cementitious property modification of basic oxygen furnace steel slag. *Constr. Build. Mater.* **2013**, *48*, 575–579. [CrossRef]
10. Wang, Q.; Yang, J.; Yan, P. Cementitious properties of super-fine steel slag. *Powder Technol.* **2013**, *245*, 35–39. [CrossRef]
11. Hou, J.; Chen, Z.; Liu, J. Hydration activity and expansibility model for the RO phase in steel slag. *Metall. Mater. Trans. B* **2020**, *51*, 1697–1704. [CrossRef]
12. Han, F.; Zhang, Z.; Wang, D.; Yan, P. Hydration heat evolution and kinetics of blended cement containing steel slag at different temperatures. *Thermochim. Acta* **2015**, *605*, 43–51. [CrossRef]
13. Pal, S.C.; Mukherjee, A.; Pathak, S.R. Investigation of hydraulic activity of ground granulated blast furnace slag in concrete. *Cem. Concr. Res.* **2003**, *33*, 1481–1486. [CrossRef]
14. Özbay, E.; Erdemir, M.; Durmuş, H.İ. Utilization and efficiency of ground granulated blast furnace slag on concrete properties–A review. *Constr. Build. Mater.* **2016**, *105*, 423–434. [CrossRef]
15. Bernal, S.A.; de Gutiérrez, R.M.; Pedraza, A.L.; Provis, J.L.; Rodriguez, E.D.; Delvasto, S. Effect of binder content on the performance of alkali-activated slag concretes. *Cem. Concr. Res.* **2011**, *41*, 1–8. [CrossRef]
16. Haha, M.B.; Le Saout, G.; Winnefeld, F.; Lothenbach, B. Influence of activator type on hydration kinetics, hydrate assemblage and microstructural development of alkali activated blast-furnace slags. *Cem. Concr. Res.* **2011**, *41*, 301–310. [CrossRef]
17. Jin, F.; Abdollahzadeh, A.; Al-Tabbaa, A. Effect of different MgO on the hydration of MgO-activated granulated ground blastfurnace slag paste. In Proceedings of the 3rd International Conference on Sustainable Construction Materials and Technologies, Kyoto, Japan, 18–21 August 2013.
18. Shen, W.; Zhou, M.; Ma, W.; Hu, J.; Cai, Z. Investigation on the application of steel slag–fly ash–phosphogypsum solidified material as road base material. *J. Hazard. Mater.* **2009**, *164*, 99–104. [CrossRef] [PubMed]
19. Shi, C.; Wu, Y. Studies on some factors affecting CO_2 curing of lightweight concrete products. *Resour. Conserv. Recycl.* **2008**, *52*, 1087–1092. [CrossRef]
20. Ghouleh, Z.; Guthrie, R.I.L.; Shao, Y. High-strength KOBM steel slag binder activated by carbonation. *Constr. Build. Mater.* **2015**, *99*, 175–183. [CrossRef]
21. Liu, J.; Ge, X.; Liu, P.; Song, G.; Hu, Z. Experimental study on the preparation of cementitious materials from iron ore tailings by activation. *Constr. Build. Mater.* **2023**, *385*, 131409. [CrossRef]
22. Rashad, A.M.; Bai, Y.; Basheer, P.A.; Milestone, N.B.; Collier, N.C. Hydration and properties of sodium sulfate activated slag. *Cem. Concr. Compos.* **2013**, *37*, 20–29. [CrossRef]
23. Zhu, X.; Hou, H.; Huang, X.; Zhou, M.; Wang, W. Enhance hydration properties of steel slag using grinding aids by mechanochemical effect. *Constr. Build. Mater.* **2012**, *29*, 476–481. [CrossRef]
24. Shi, C. Characteristics and cementitious properties of ladle slag fines from steel production. *Cem. Concr. Res.* **2002**, *32*, 459–462. [CrossRef]
25. Yan, J.; Wu, S.; Yang, C.; Zhao, Z.; Xie, J. Influencing mechanisms of RO phase on the cementitious properties of steel slag powder. *Constr. Build. Mater.* **2022**, *350*, 128926. [CrossRef]
26. Mehdizadeh, H.; Jia, X.; Mo, K.H.; Ling, T.C. Effect of water-to-cement ratio induced hydration on the accelerated carbonation of cement pastes. *Environ. Pollut.* **2021**, *280*, 116914. [CrossRef]
27. Zhong, X.; Li, L.; Jiang, Y.; Ling, T.C. Elucidating the dominant and interaction effects of temperature, CO2 pressure and carbonation time in carbonating steel slag blocks. *Constr. Build. Mater.* **2021**, *302*, 124158. [CrossRef]
28. Gu, X.; Ge, X.; Liu, J.; Song, G.; Wang, S.; Hu, Z.; Wang, H. Study on the synergistic effect of calcium carbide residue-fly ash enhanced desulphurisation gypsum under high temperature maintenance condition. *Constr. Build. Mater.* **2024**, *412*, 134706. [CrossRef]
29. Liu, J.; Song, G.; Ge, X.; Liu, B.; Liu, K.; Tian, Y.; Wang, X.; Hu, Z. Experimental Study on the Properties and Hydration Mechanism of Gypsum-Based Composite Cementitious Materials. *Buildings* **2024**, *14*, 314. [CrossRef]
30. Zhao, J.; Wang, D.; Yan, P.; Zhang, D.; Wang, H. Self-cementitious property of steel slag powder blended with gypsum. *Constr. Build. Mater.* **2016**, *113*, 835–842. [CrossRef]
31. Chen, S.; Yuan, H. Characterization and optimization of eco-friendly cementitious materials based on titanium gypsum, fly ash, and calcium carbide residue. *Constr. Build. Mater.* **2022**, *349*, 128635. [CrossRef]
32. Chen, Z.; Ye, H. The role of CaO and MgO incorporation in chloride resistance of sodium carbonate-activated slag. *Cem. Concr. Compos.* **2022**, *132*, 104625. [CrossRef]
33. Abdalqader, A.F.; Jin, F.; Al-Tabbaa, A. Characterisation of reactive magnesia and sodium carbonate-activated fly ash/slag paste blends. *Constr. Build. Mater.* **2015**, *93*, 506–513. [CrossRef]
34. Zhao, J.; Li, Z.; Wang, D.; Yan, P.; Luo, L.; Zhang, H.; Zhang, H.; Gu, X. Hydration superposition effect and mechanism of steel slag powder and granulated blast furnace slag powder. *Constr. Build. Mater.* **2023**, *366*, 130101. [CrossRef]
35. Duan, S.; Liao, H.; Cheng, F.; Song, H.; Yang, H. Investigation into the synergistic effects in hydrated gelling systems containing fly ash, desulfurization gypsum and steel slag. *Constr. Build. Mater.* **2018**, *187*, 1113–1120. [CrossRef]
36. Han, F.; Zhou, Y.; Zhang, Z. Effect of gypsum on the properties of composite binder containing high-volume slag and iron tailing powder. *Constr. Build. Mater.* **2020**, *252*, 119023. [CrossRef]
37. Jin, F.; Gu, K.; Al-Tabbaa, A. Strength and drying shrinkage of reactive MgO modified alkali-activated slag paste. *Constr. Build. Mater.* **2014**, *51*, 395–404. [CrossRef]

38. Wang, Q.; Yan, P. Hydration properties of basic oxygen furnace steel slag. *Constr. Build. Mater.* **2010**, *24*, 1134–1140. [CrossRef]
39. Cui, X.; Ni, W. Hydration behavior of cementitious materials with all solid waste based of steel slag and blast furnace slag. *Rev. Fac. Ing.* **2016**, *31*, 172–181.

Disclaimer/Publisher's Note: The statements, opinions and data contained in all publications are solely those of the individual author(s) and contributor(s) and not of MDPI and/or the editor(s). MDPI and/or the editor(s) disclaim responsibility for any injury to people or property resulting from any ideas, methods, instructions or products referred to in the content.